HHS Public Access

Author manuscript

Nat Genet. Author manuscript; available in PMC 2013 June 10.

Published in final edited form as:

Nat Genet. ; 44(4): 440–S2. doi:10.1038/ng.1091.

De novo mutations in the actin genes *ACTB* and *ACTG1* cause Baraitser-Winter syndrome

Jean-Baptiste Rivière[1,*], **Bregje W M van Bon**[2,*], **Alexander Hoischen**[2], **Stanislav S Kholmanskikh**[3], **Brian J O'Roak**[4], **Christian Gilissen**[2], **Sabine Gijsen**[2], **Christopher T Sullivan**[1], **Susan L Christian**[1], **Omar A Abdul-Rahman**[5], **Joan F Atkin**[6], **Nicolas Chassaing**[7], **Valerie Drouin-Garraud**[8], **Andrew E Fry**[9], **Jean-Pierre Fryns**[10], **Karen W Gripp**[11], **Marlies Kempers**[2], **Tjitske Kleefstra**[2], **Grazia M S Mancini**[12], **Małgorzata J M Nowaczyk**[13], **Conny M A van Ravenswaaij-Arts**[14], **Tony Roscioli**[2], **Michael Marble**[15], **Jill A Rosenfeld**[16], **Victoria M Siu**[17], **Bert B A de Vries**[2], **Jay Shendure**[4], **Alain Verloes**[18], **Joris A Veltman**[2], **Han G Brunner**[2], **M Elizabeth Ross**[3], **Daniela T Pilz**[9,*], and **William B Dobyns**[1,19,*]

[1]Center for Integrative Brain Research, Seattle Children's Hospital, Seattle, WA [2]Department of Human Genetics, Radboud University Nijmegen Medical Centre, Nijmegen, The Netherlands [3]Department of Neurology and Neuroscience, Weill Medical College of Cornell University, New York, NY [4]Department of Genome Sciences, University of Washington, Seattle, WA [5]Department of Pediatrics, University of Mississippi Medical Center, Jackson, MS [6]Department of Pediatrics, College of Medicine, Ohio State University, Columbus, OH [7]Department of Medical Genetics, Toulouse University Hospital and Toulouse III Paul-Sabatier University, Toulouse, France [8]Department of Genetics, University Hospital, Rouen, France [9]Institute of Medical Genetics, University Hospital of Wales, Cardiff, UK [10]Departement Menselijke Erfelijkheid, Center for Human Genetics, University Hospital Leuven, Leuven, Belgium [11]Division of Medical Genetics, A. I. duPont Hospital for Children, Wilmington, DE [12]Department of Clinical Genetics, Erasmus Medical Center, Rotterdam, The Netherlands [13]Department of Pathology and Molecular Medicine, McMaster University, Hamilton, ON, Canada [14]Department of Genetics, University Medical

Corresponding authors: Daniela T. Pilz, M.D., Institute of Medical Genetics, University Hospital of Wales, Cardiff CF14 4XW, UK, Phone: +44 (0)2920744038, Fax: +44 (0)2920743863, Daniela.Pilz@wales.nhs.uk. William B. Dobyns, M.D., Seattle Children's Research Institute, Center for Integrative Brain Research, 1900 Ninth Avenue, M/S C9S-10, Seattle WA 98101, USA, Phone: 1-206-884-2972, Fax: 1-206- 206-884-1210, wbd@uw.edu.

*Denotes equal contribution.

Data access

The whole-exome sequencing data from individuals of trio 1 have been deposited in dbGaP under accession number (pending).

Author Contributions

D.T.P., W.B.D., A.V. and H.G.B. designed the study. J.B.R., B.W.M.v.B. and A.H. designed and performed the genetics experiments. S.S.K. performed the experiments in lymphoblastoid cell lines. J.B.R., A.H., B.J.O. and C.G. performed the bioinformatics experiments. B.J.O. analyzed the control exome datasets. S.G. contributed to the genetics experiments. C.T.S. and S.L.C. prepared DNA samples and lymphoblastoid cell lines. O.A.A.R., J.F.A., N.C., V.D.G., A.E.F., J.P.F., K.W.G., M.K., T.K., G.M.S.M., M.J.M.N., C.M.A.v.R.A., T.R., B.B.A.d.V., M.M., V.M.S., A.V., H.G.B., D.T.P. and W.B.D. recruited and evaluated the study subjects. J.A.R. analyzed the Signature Genomic Laboratories dataset. J.S. supervised B.J.O., J.A.V. supervised A.H., C.G. and S.G., H.G.B. supervised B.W.M.v.B., M.E.R. supervised and evaluated data with S.S.K. and wrote sections dealing with lymphoblastoid cell lines, and W.B.D. supervised J.B.R.. J.B.R. and W.B.D. wrote the paper.

Competing financial interests

The authors report no competing financial interests.

Center Groningen, University of Groningen, Groningen, The Netherlands [15]Department of Pediatrics, Louisiana State University Health Sciences Center and Children's Hospital of New Orleans, New Orleans, LA [16]Signature Genomic Laboratories, PerkinElmer, Inc., Spokane, WA [17]Department of Pediatrics, University of Western Ontario, London, ON, Canada [18]Département de Génétique, Hôpital Robert Debré, Paris, France [19]Departments of Pediatrics and Neurology, University of Washington, Seattle, WA

Abstract

Brain malformations are individually rare but collectively common causes of developmental disabilities[1–3]. Many forms occur sporadically and have reduced reproductive fitness, pointing towards a causative role for *de novo* mutations[4,5]. Here we report our studies of Baraitser-Winter syndrome, a well-defined syndrome characterized by distinct craniofacial features, ocular colobomata and a neuronal migration defect[6,7]. By using whole-exome sequencing in three proband-parent trios, we identified *de novo* missense changes in the cytoplasmic actin genes *ACTB* and *ACTG1* in one and two probands, respectively. Sequencing of both genes in fifteen additional patients revealed disease-causing mutations in all probands, including two recurrent *de novo* mutations (*ACTB* p.Arg196His and *ACTG1* p.Ser155Phe). Our results confirm that trio-based exome sequencing is a powerful approach to discover the genes causing sporadic developmental disorders, emphasize the overlapping roles of cytoplasmic actins in development, and suggest that Baraitser-Winter syndrome is the predominant phenotype associated with mutations of these two genes.

Whole-exome sequencing has recently been used to detect disease-causing mutations underlying rare sporadic syndromes in just a few unrelated individuals[8–10]. However, this becomes more difficult in the presence of any locus heterogeneity. For disorders hypothesized to result from *de novo* mutations, a potentially more powerful alternative approach involves exome sequencing in parent-child trios, which should rapidly narrow the number of candidate mutations to a handful in view of the rarity of *de novo* events in protein coding sequences[11,12]. This strategy has been successfully applied to identify *de novo* point mutations in intellectual disability[4], autism[13], and schizophrenia[14,15].

Baraitser-Winter syndrome is a rare but well-defined developmental disorder recognized by the combination of congenital ptosis, high-arched eyebrows, hypertelorism, ocular colobomata and a brain malformation consisting of anterior predominant lissencephaly. Other typical features include postnatal short stature and microcephaly, intellectual disability, seizures and hearing loss[6,7,16–18]. Neither familial recurrence nor consanguinity have been observed in any families including the 18 reported here (Supplementary note), and chromosome microarrays have not detected any pathogenic copy number variants (CNVs). We therefore hypothesized that the genetic basis of Baraitser-Winter syndrome was likely to result from *de novo* point mutations and performed whole-exome sequencing in three probands (patient LP98-083 is shown in Fig. 1) and their unaffected parents using two different platforms. Exome capture and sequencing were performed using NimbleGen solution-based capture and Illumina sequencing for trio 1 (LP98-083), and Agilent

SureSelect target enrichment system with ABI SOLiD sequencing for trios 2 (58248) and 3 (58431) (**Online Methods**). Both platforms generated a coverage of at least ten reads for more than 85% of the targeted exome and we identified 22,591 to 29,685 genetic variants per proband (Table 1). As previously described[4,13], we filtered variants to systematically identify candidate *de novo* events in each proband. Given the severe phenotype, we focused on protein-altering and splice-site variants absent from other exome datasets available locally or from the dbSNP or 1000 Genomes Project databases[19]. Similar to previous studies[4,13–15], we identified two to six candidate *de novo* mutations per proband (Table 1 and Supplementary Table 1), all of which were tested by Sanger sequencing.

The two sequencing and analysis platforms converged to identify *de novo* missense changes in the cytoplasmic γ-actin gene *ACTG1* (NM_001614.2) in two probands and in the β-actin gene *ACTB* (NM_001101.2) in the third (Supplementary Fig. 1). We used Sanger sequencing to screen the coding sequence of both genes in 15 additional patients and detected pathogenic mutations in all. Altogether, we found 10 and 8 mutations in *ACTB* and *ACTG1*, respectively (Table 2). These proved to be *de novo* in all 11 subjects with parental DNA available, and 6 of 7 remaining mutations were identical to mutations shown to be *de novo* in the first group. Strikingly, 8 patients (44%) carried a mutation disrupting Arg196 of β-actin, including 7 with the same nucleotide change (c.587G>A, p.Arg196His). These recurrent transitions occurred at a CpG dinucleotide, which is known to be susceptible to deamination of methylcytosines[20], thus suggesting a possible mechanism for the high frequency of this mutation. Another 3 (17%) had a mutation disrupting Ser155 of cytoplasmic γ-actin.

Several control datasets were analyzed to validate our findings and assess the number of coding variants in *ACTB* and *ACTG1*. These included whole-exome sequence data from 244 unrelated healthy individuals of European descent (**Online Methods** and Supplementary Table 2) and genome-wide sequence data from 629 and ~2,500 individuals available from the 1000 Genomes Pilot Project[19] and NHLBI Exome Sequencing Project (ESP) websites (Supplementary Tables 3 and 4). None of the mutations identified in Baraitser-Winter syndrome patients were present in this large dataset. Further, no CNVs encompassing *ACTB* or *ACTG1* exons were observed in 2,349 control individuals (**Online Methods**). The ESP dataset showed a striking ratio of synonymous to non-synonymous substitutions of 79:1 for the covered portion of *ACTB* and *ACTG1* combined. On a genome-wide scale[19], this ratio is estimated at ~1:1, thus indicating strong selection against non-synonymous mutations in both genes. Surprisingly, one of the *ACTG1 de novo* mutations (p.Ala135Val) was recorded in dbSNP (rs11549190, Table 2). This variant was originally identified, but not validated, from large-scale sequencing of expressed sequence tags[21]. Given its absence in the aforementioned datasets, we concluded that this report was likely an error in dbSNP.

Actins are a family of essential cytoskeletal proteins implicated in nearly all cellular processes[22–25]. Among the six human genes encoding actins, only *ACTB* and *ACTG1* are ubiquitously expressed; the remaining four are expressed primarily in muscle. The cytoplasmic β- and γ-actins are highly conserved throughout evolution and nearly identical to each other, differing by only four amino acids[26] (Supplementary Fig. 2). Despite their striking homology and presence in all cell types[27], β- and γ-actins have been proposed to

play at least partially distinct physiological functions based on their relative spatial and temporal enrichment in neurons[28] and other cell types[29,30], and on different phenotypes observed in homozygous mouse mutants. *Actb*$^{-/-}$ is embryonically lethal, while *Actg1*$^{-/-}$ shows reduced viability with some surviving to adulthood[25,31,32]. Previously reported heterozygous *ACTB* and *ACTG1* mutations in humans also suggest a more severe phenotype for *ACTB* mutations[33–35] (phenotype reviewed in Supplementary note and Supplementary Table 5). In contrast, our findings suggest that both isoforms have significant overlapping but non-redundant functions during human development, as illustrated by the indistinguishable clinical presentation of Baraitser-Winter syndrome patients carrying mutations in *ACTB* and *ACTG1* (Table 3 and Supplementary Table 6).

Protein levels and morphology of lymphoblastoid cell lines from six affected individuals were examined, representative examples of which appear in Fig. 2 and 3. No change in protein levels of β- and γ-actin were seen between these two cell lines (Fig. 2) or four additional mutant lines and controls (Supplementary Fig. 3), similar to one previously reported *ACTB* mutation[34]. Both mutant lines derived from patients carrying one or the other of the two *ACTB* and *ACTG1* recurrent mutations (p.Arg196His and p.Ser155Phe, Fig. 3) contained greatly increased F-actin content and multiple anomalous F-actin rich filopodia-like protrusions compared to control cells, resulting in an increased cell perimeter (Fig. 3b). The stability of F-actin in these cells was probed using latrunculin A, which binds actin monomers thereby preventing their incorporation into growing filaments[36]. Both mutant lines showed altered sensitivity to latrunculin A, albeit with different outcomes. We observed an increased resistance to latrunculin A in β-actin p.Arg196His mutant cells, which is consistent with the previously reported p.Arg183Trp mutation[34], whereas the γ-actin p.Ser155Phe mutant displayed increased sensitivity to the treatment (Fig. 3c). Immunofluorescent staining of F-actin in lymphoblastoid cell lines from four additional patients showed patterns of cytoskeletal changes and abnormal accumulation of F-actin that were reproducible between independent cell lines carrying the same mutation (p.Arg196His in LR04-173 and LR09-079; p.Ser155Phe in LP98-096 and LR04-298, Fig. 3 and Supplementary Fig. 4). Consistent with our initial analysis of p.Arg196His and p.Ser155Phe mutant lines, all mutants examined presented striking yet distinct patterns of abnormal F-actin organization, suggesting that morphologies are mutation specific. Altogether, our data indicate that mutations associated with Baraitser-Winter syndrome result in increased F-actin content and altered F-actin dynamics in response to latrunculin A treatment. These effects should impact cell morphology, motility, and other actin-related functions.

Several observations support a dominant-negative or gain-of-function mechanism for the disease-causing mutations. Firstly, none of our subjects had deletions or protein-truncating mutations, which are an indication of haploinsufficiency. Further, 11 of 18 mutations (61%) disrupt the same two amino-acids (*ACTB* Arg196 and *ACTG1* Ser155). Although these could be hypermutable sites, mutation clustering suggests a gain-of-function effect, as observed in Noonan[37], FGFR-related craniosynostosis[38] and Proteus syndromes[39]. Second, patients with complete deletion or duplication of *ACTB* do not have Baraitser-Winter syndrome. To assess the latter, we searched the databases of two large clinical laboratories performing chromosome microarrays, Signature Genomic Laboratories and the Department

of Human Genetics, Radboud University Nijmegen Medical Centre, and ascertained four children: two with a deletion and one with a duplication of 7p22 that included *ACTB*, and one with a deletion of 17q25.3 that included *ACTG1*. All lacked the major and most severe features of Baraitser-Winter syndrome, which are congenital ptosis and high-arched eyebrows, neuronal migration malformation and colobomata (Supplementary note and Supplementary Fig. 5). Finally, the unchanged β- and γ-actin protein levels coupled with increased F-actin content observed in patient-derived lymphoblastoid cell lines also argue against haploinsufficiency.

In conclusion, our results show that Baraitser-Winter syndrome is a clinically well-defined syndrome caused by mutations in the cytoplasmic actin genes *ACTB* and *ACTG1* and provide additional evidence that actin plays a central role in the pathogenesis of lissencephaly[40,41]. Our data also show that even in a scenario of limited genetic heterogeneity, whole-exome sequencing of a small number of trios combined with validation in additional patients is a powerful approach to identify mutations underlying well-defined sporadic disorders, especially those with low reproductive fitness. Because mutations of either *ACTB* or *ACTG1* cause an indistinguishable phenotype, we hypothesize that mutations observed in Baraitser-Winter syndrome affect developmental functions shared by cytoplasmic β- and γ-actins. Functional comparison of mutations identified in Baraitser-Winter syndrome and other actinopathies should help elucidate both the distinct and overlapping functions of cytoplasmic β- and γ-actin isoforms. We conclude that Baraitser-Winter syndrome comprises the severe end of the predominant phenotype spectrum associated with mutations of both *ACTB* and *ACTG1*, a spectrum that extends from Baraitser-Winter syndrome to non-syndromic hearing loss.

METHODS

Subjects

Written, informed consent was obtained from all subjects prior to enrollment in the study. Experiments on human subjects were approved by institutional review boards at all participating institutions. The study included 18 unrelated patients; the diagnosis of Baraitser-Winter syndrome was based on previously reported clinical features[6,7,17,18], and review of MRI brain scans when available. Genomic DNA was extracted from whole-blood or saliva using standard methods. When parental DNA was available, paternity-maternity testing was performed by genotyping a panel of polymorphic short tandem repeats.

Exome sequencing

Trio 1—Five micrograms of whole-blood genomic DNA from the affected proband and his parents were sent to the University of Washington Genome Sciences Genomic Resource Center for exome capture and sequencing. Whole-exome sequence capture was performed using the SeqCap EZ Exome Library v2.0 liquid phase sequence capture kit (Roche). Libraries were then sequenced on an Illumina Genome Analyzer IIx according to the manufacturer's recommendations for paired-end 76-bp reads. On average, we generated 81 million total reads (68 million mapped reads) and 5.2 gigabases (Gb) of mappable sequence per individual. We aligned reads to the human reference genome (hg19) with the Burrows-

Wheeler Aligner (BWA)[42] and removed potential duplicate paired-end reads. The Genome Analysis Toolkit (GATK)[43,44] was used for base quality score recalibration and indel realignment as well as for single nucleotide variant and indel discovery and genotyping using standard hard filtering parameters[43]. Variants with quality scores < 30, allele balance > 0.75, sequencing depth < 4, quality/depth ratio < 5.0, length of homopolymer run > 5.0, and strand bias > −0.10 were flagged and excluded from subsequent analyses. Coverage was assessed with the GATK Depth of Coverage tool by ignoring reads with mapping quality < 20 and bases with base quality < 30. 92% of the primary target was covered ≥ 4 times in all three individuals.

Trios 2 and 3

Massively parallel sequencing of genomic DNA from two patient-parent trios was performed at the Radboud University Nijmegen Medical Center by using the ABI SOLiD™ 4 platform (Life Technologies). Enrichment of exonic sequences was achieved by using the 50 Mb human SureSelect set (Agilent), which targets ~21,000 human genes. On average, we obtained > 120 million mappable sequencing reads and 4.6 Gb of mappable sequence data per individual after multiplex sequencing, using 4 exomes per sequencing slide. Colour space reads were mapped to the hg19 reference genome with the SOLiD bioscope software version 1.3, which utilizes an iterative mapping approach. On average, 81% of bases originated from the targeted exome, resulting in a mean coverage of 88-fold (median 66-fold). 88% of the targeted exons were covered more than 10 times. Single nucleotides variants were subsequently called by the DiBayes algorithm using high stringency calling settings and small insertions and deletions were detected using the SOLiD Small Indel Tool.

Discovery of *de novo* candidate variants

Trio 1—The 22,591 variants identified in the patient were annotated with SeattleSeq SNP annotation (http://snp.gs.washington.edu/SeattleSeqAnnotation131/). We focused on protein-altering variants (missense, nonsense, splice-site variants, and coding indels) absent from dbSNP (build 132), 1000 Genomes Project data[19], and 101 other exomes. From this list of rare variants, we identified potential *de novo* events using the following parameters: presence of ≥ 2 variant reads in the proband, sequencing depth at the variant position ≥ 4 in both parents, and parental allelic balance > 0.90. Evolutionary conservation at the nucleotide level and impact of amino acid substitutions were assessed using the Genomic Evolutionary Rate Profiling (GERP)[45] and Grantham matrix scores[46], respectively. Candidate *de novo* events were then inspected using IGV[47] and validated in all three individuals by standard PCR reactions using custom primers designed with Primer3 (http://frodo.wi.mit.edu/primer3/) and Sanger sequencing.

Trios 2 and 3—A total of 28,497 and 29,685 variants were identified in probands of trio 2 (58248) and trio 3 (58431), respectively. All variants were annotated using an in-house annotation pipeline built in Nijmegen, as previously reported[4,8,9,48]. These variants were filtered and analyzed for potential *de novo* occurrence using an automated prioritization scheme[4] involving an automated check of all private non-synonymous variants identified in the patients for occurrence in the respective parental bam files. Candidate *de novo* events were then verified using conventional Sanger sequencing.

Control exomes

For trio 1, variants were compared against 101 other exomes sequenced at the University of Washington, including 88 exomes from the NIEHS SNPs project (http://snp.gs.washington.edu/niehsExome/), and 13 exomes sequenced in the same batch as the trio and consisting of healthy individuals and patients with unrelated disorders. For trios 2 and 3, we used 332 other exomes sequenced at the Radboud University Nijmegen Medical Center to remove systematic artifacts and low-frequency variants.

We also analyzed the coding exons (+/− 2 bp) of *ACTB* and *ACTG1* in exome sequence data from 244 unrelated healthy individuals of European descent, which consist of parents of children with sporadic autism. These samples were sequenced at the University of Washington Genome Sciences using SeqCap EZ Exome Library v2.0 (Roche) and the Illumina sequencing platform. For all control samples combined, 89% of the bases of *ACTB* and *ACTG1* were covered ≥ 8x. The average per-base coverage was 23x and 31x for *ACTB* and *ACTG1*, respectively. The first coding exon of *ACTB* had a low read depth, with an average coverage of 4x; all other exons had sufficient coverage to call variants in the majority of samples. Variants were filtered to 8x coverage and consensus or variant quality of 30 using SAMtools[49], as previously described[13].

Identification of copy number variations (CNV) in control individuals

Genomic DNA samples from 2,349 control individuals (including 1,953 of European ancestry) were genotyped using the InfiniumII HumanHap610 Quad BeadChip array (Illumina) at the Center for Applied Genomics at Children's Hospital of Philadelphia. Control subjects consisted of 0–18 years of age healthy children that were primarily recruited from the Philadelphia region through the Hospital's Health Care Network. Copy number variations were identified using the PennCNV algorithm[50] and further filtered using a threshold of 10 consecutive single nucleotide variants, a length of 30 kilobase pairs, and a PennCNV confidence score of 10.

Sanger sequencing

We amplified the coding and flanking intronic regions of the *ACTG1* (NM_001614.2) and *ACTB* (NM_001101.2) genes in genomic DNA from 18 probands. PCR products were sequenced at the University of Washington High-Throughput Genomics Unit or the Radboud University Nijmegen Medical Centre. All mutations were confirmed by reamplification of the fragment and resequencing of the proband and his or her available relatives. Primer sequences and PCR conditions are available on request.

SDS-PAGE, Coomassie staining and Western Blot

Epstein-Barr virus immortalized lymphoblastoid cell lines were established from peripheral blood samples of six affected individuals (LR04-173, LP98-096, LR09-079, LP98-085, LR04-298 and LR06-241) and two control individuals (09.1359 and 07.0841) using standard procedures. Cells were collected from suspension culture by centrifugation at 1,000 g for 10 min. Cell pellets were rinsed once with PBS and lysed in M-PER lysis buffer (Pierce) supplemented with protease and phosphatase inhibitor cocktail (Sigma). Protein

concentration of the lysates cleared of insoluble cell debris were determined using 660 nm Protein Assay reagent (Pierce) and more concentrated samples were diluted to the concentration of the least concentrated sample with the lysis buffer. For SDS-PAGE equal volumes of concentration-adjusted lysates were mixed with LDS electrophoresis loading buffer (Life Technologies), then reduced and denatured for 10 min at +70°C. For 1D electrophoresis equal volumes of reduced denatured samples were separated on two 4–12% polyacrylamide gels (Life Technologies). One of the gels was processed for Coomassie staining (Bio-Rad), as per manufacturer's recommendations. The other gel was transferred onto 0.2 μm nitrocellulose membrane (Pall) and processed for Western Blotting. Primary antibodies for Western Blotting were used at the following dilutions: mouse anti-ACTB (clone AC-15, Sigma, 1:32,000), mouse anti-ACTG1 (clone 2–2.1.14.17, Sigma, 1:16,000), and goat anti-GAPDH (Santa-Cruz biotechnology, 1:1,000). Appropriate secondary HRP-conjugated antibodies (Bio-Rad) were used at 1:40,000. Proteins were detected by incubation with chemiluminescent substrate SuperSignal Pico (Pierce), as per manufacturer's protocol. Appropriate secondary HRP-conjugated antibodies (Bio-Rad) were used at 1:40,000. Proteins were detected by incubation with chemiluminescent substrate SuperSignal Pico (Pierce), as per manufacturer's protocol.

Immunofluorescent staining of actin in cultured cells

Lymphoblastoid cells grown in suspension were placed on fibronectin (Millipore, 100 μg/ml) and laminin (Invitrogen, 25 μg/ml) coated glass cover slips for 2 hr. After cells attached, experimental cultures were treated with Latrunculin A (Cayman Chemical Company, 0.6 μM) for 2 hr. Immediately after treatment, cells were fixed with 0.25% glutaraldehyde and permeabilized with 0.1% triton x100. Mouse anti-α-tubulin primary antibody (Sigma, 1:5,000) was applied for overnight at +4°C. Secondary AlexaFluor-conjugated antibody (Life Technologies, 1:1,000) along with AlexaFluor-conjugated phalloidin to visualize F-actin (Life Technologies, 1:100) were applied for 1 hr at room temperature. Cover glasses were mounted in ProLong anti-fade media (Life Technologies) and visualized with 100x oil objective on inverted microscope (Zeiss) fitted with spinning disc confocal scanner (Perkin-Elmer). All imaging analysis was performed using ImageJ software as follows. Confocal stacks were projected into a single plane (Z-project, Maximal Intensity). Images were thresholded, perimeter was measured as object perimeter and fluorescence intensity measured as a mean gray value.

Supplementary Material

Refer to Web version on PubMed Central for supplementary material.

Acknowledgments

We would like to thank the families for their contribution to this study. We thank all members of the Northwest Genomics Center and Genomic Disorders Group Nijmegen, as well as personnel from the Microarray Facility and Sequencing Facility Nijmegen for excellent technical assistance. This work was supported by the US National Institutes of Health (grants 1R01-NS058721 to W.B.D. and 2PO1-NS048120 to M.E.R.), the Netherlands Organization for Health Research and Development (ZonMW grants 917-66-363 and 911-08-025 to J.A.V.), the EU-funded TECHGENE project (Health-F5-2009-223143 to J.A.V.) and the AnEUploidy project (LSHG-CT-2006-37627 to A.H., B.W.M.v.B., H.G.B. and J.A.V.). J.B.R. is supported by a Banting Postdoctoral Fellowship from the Canadian Institutes of Health Research. T.R. is supported by an Australian NHMRC post-

doctoral fellowship. We would like to thank the Simons Foundation Autism Research Initiative (SFARI) that provided control exome data (grant 191889), the NIEHS Environmental Genome Project for providing support for this project (contract No.HHSN273200800010C), and the NHLBI GO Exome Sequencing Project and its ongoing studies which produced and provided exome variant calls for comparison: the Lung GO Sequencing Project (HL-102923), the WHI Sequencing Project (HL-102924), the Broad GO Sequencing Project (HL-102925), the Seattle GO Sequencing Project (HL-102926) and the Heart GO Sequencing Project (HL-103010).

References

1. Glinianaia SV, Rankin J, Colver A. Cerebral palsy rates by birth weight, gestation and severity in North of England, 1991–2000 singleton births. Arch Dis Child. 2011; 96:180–185. [PubMed: 21068077]
2. Rankin J, et al. Congenital anomalies in children with cerebral palsy: a population-based record linkage study. Dev Med Child Neurol. 2010; 52:345–351. [PubMed: 19737295]
3. von Wendt L, Rantakallio P. Congenital malformations of the central nervous system in a 1-year birth cohort followed to the age of 14 years. Childs Nerv Syst. 1986; 2:80–82. [PubMed: 2942247]
4. Vissers LE, et al. A de novo paradigm for mental retardation. Nat Genet. 2010; 42:1109–1112. [PubMed: 21076407]
5. Cooper GM, et al. A copy number variation morbidity map of developmental delay. Nat Genet. 2011; 43:838–846. [PubMed: 21841781]
6. Baraitser M, Winter RM. Iris coloboma, ptosis, hypertelorism, and mental retardation: a new syndrome. J Med Genet. 1988; 25:41–43. [PubMed: 3351890]
7. Ramer JC, et al. Previously apparently undescribed syndrome: shallow orbits, ptosis, coloboma, trigonocephaly, gyral malformations, and mental and growth retardation. Am J Med Genet. 1995; 57:403–409. [PubMed: 7545868]
8. Hoischen A, et al. De novo mutations of SETBP1 cause Schinzel-Giedion syndrome. Nat Genet. 2010; 42:483–485. [PubMed: 20436468]
9. Hoischen A, et al. De novo nonsense mutations in ASXL1 cause Bohring-Opitz syndrome. Nat Genet. 2011; 43:729–731. [PubMed: 21706002]
10. Ng SB, et al. Exome sequencing identifies MLL2 mutations as a cause of Kabuki syndrome. Nat Genet. 2010; 42:790–793. [PubMed: 20711175]
11. Conrad DF, et al. Variation in genome-wide mutation rates within and between human families. Nat Genet. 2011; 43:712–714. [PubMed: 21666693]
12. Lynch M. Rate, molecular spectrum, and consequences of human mutation. Proc Natl Acad Sci U S A. 2010; 107:961–968. [PubMed: 20080596]
13. O'Roak BJ, et al. Exome sequencing in sporadic autism spectrum disorders identifies severe de novo mutations. Nat Genet. 2011; 43:585–589. [PubMed: 21572417]
14. Girard SL, et al. Increased exonic de novo mutation rate in individuals with schizophrenia. Nat Genet. 2011; 43:860–863. [PubMed: 21743468]
15. Xu B, et al. Exome sequencing supports a de novo mutational paradigm for schizophrenia. Nat Genet. 2011; 43:864–868. [PubMed: 21822266]
16. Fryns JP, Aftimos S. New MR/MCA syndrome with distinct facial appearance and general habitus, broad and webbed neck, hypoplastic inverted nipples, epilepsy, and pachygyria of the frontal lobes. J Med Genet. 2000; 37:460–462. [PubMed: 10928857]
17. Rossi M, Guerrini R, Dobyns WB, Andria G, Winter RM. Characterization of brain malformations in the Baraitser-Winter syndrome and review of the literature. Neuropediatrics. 2003; 34:287–292. [PubMed: 14681753]
18. Verloes A. Iris coloboma, ptosis, hypertelorism, and mental retardation: Baraitser-Winter syndrome or Noonan syndrome? J Med Genet. 1993; 30:425–426. [PubMed: 8320709]
19. A map of human genome variation from population-scale sequencing. Nature. 2010; 467:1061–1073. [PubMed: 20981092]
20. Scarano E, Iaccarino M, Grippo P, Parisi E. The heterogeneity of thymine methyl group origin in DNA pyrimidine isostichs of developing sea urchin embryos. Proc Natl Acad Sci U S A. 1967; 57:1394–1400. [PubMed: 5231746]

21. Buetow KH, Edmonson MN, Cassidy AB. Reliable identification of large numbers of candidate SNPs from public EST data. Nat Genet. 1999; 21:323–325. [PubMed: 10080189]
22. Gupton SL, Gertler FB. Filopodia: the fingers that do the walking. Sci STKE 2007. 2007:re5.
23. Harborth J, Elbashir SM, Bechert K, Tuschl T, Weber K. Identification of essential genes in cultured mammalian cells using small interfering RNAs. J Cell Sci. 2001; 114:4557–4565. [PubMed: 11792820]
24. Lambrechts A, Van Troys M, Ampe C. The actin cytoskeleton in normal and pathological cell motility. Int J Biochem Cell Biol. 2004; 36:1890–1909. [PubMed: 15203104]
25. Shawlot W, Deng JM, Fohn LE, Behringer RR. Restricted beta-galactosidase expression of a hygromycin-lacZ gene targeted to the beta-actin locus and embryonic lethality of beta-actin mutant mice. Transgenic Res. 1998; 7:95–103. [PubMed: 9608737]
26. Vandekerckhove J, Weber K. At least six different actins are expressed in a higher mammal: an analysis based on the amino acid sequence of the amino-terminal tryptic peptide. J Mol Biol. 1978; 126:783–802. [PubMed: 745245]
27. Garrels JI, Gibson W. Identification and characterization of multiple forms of actin. Cell. 1976; 9:793–805. [PubMed: 1017015]
28. Yao J, Sasaki Y, Wen Z, Bassell GJ, Zheng JQ. An essential role for beta-actin mRNA localization and translation in Ca2+-dependent growth cone guidance. Nat Neurosci. 2006; 9:1265–1273. [PubMed: 16980965]
29. Dugina V, Zwaenepoel I, Gabbiani G, Clement S, Chaponnier C. Beta and gamma-cytoplasmic actins display distinct distribution and functional diversity. J Cell Sci. 2009; 122:2980–2988. [PubMed: 19638415]
30. Hofer D, Ness W, Drenckhahn D. Sorting of actin isoforms in chicken auditory hair cells. J Cell Sci. 1997; 110 (Pt 6):765–770. [PubMed: 9099950]
31. Belyantseva IA, et al. Gamma-actin is required for cytoskeletal maintenance but not development. Proc Natl Acad Sci U S A. 2009; 106:9703–9708. [PubMed: 19497859]
32. Bunnell TM, Ervasti JM. Delayed embryonic development and impaired cell growth and survival in Actg1 null mice. Cytoskeleton (Hoboken). 2010; 67:564–572. [PubMed: 20662086]
33. Nunoi H, et al. A heterozygous mutation of beta-actin associated with neutrophil dysfunction and recurrent infection. Proc Natl Acad Sci U S A. 1999; 96:8693–8698. [PubMed: 10411937]
34. Procaccio V, et al. A mutation of beta -actin that alters depolymerization dynamics is associated with autosomal dominant developmental malformations, deafness, and dystonia. Am J Hum Genet. 2006; 78:947–960. [PubMed: 16685646]
35. Zhu M, et al. Mutations in the gamma-actin gene (ACTG1) are associated with dominant progressive deafness (DFNA20/26). Am J Hum Genet. 2003; 73:1082–1091. [PubMed: 13680526]
36. Yarmola EG, Somasundaram T, Boring TA, Spector I, Bubb MR. Actin-latrunculin A structure and function. Differential modulation of actin-binding protein function by latrunculin A. J Biol Chem. 2000; 275:28120–28127. [PubMed: 10859320]
37. Tartaglia M, Gelb BD. Noonan syndrome and related disorders: genetics and pathogenesis. Annu Rev Genomics Hum Genet. 2005; 6:45–68. [PubMed: 16124853]
38. Ibrahimi OA, Zhang F, Eliseenkova AV, Linhardt RJ, Mohammadi M. Proline to arginine mutations in FGF receptors 1 and 3 result in Pfeiffer and Muenke craniosynostosis syndromes through enhancement of FGF binding affinity. Hum Mol Genet. 2004; 13:69–78. [PubMed: 14613973]
39. Lindhurst MJ, et al. A mosaic activating mutation in AKT1 associated with the Proteus syndrome. N Engl J Med. 2011; 365:611–619. [PubMed: 21793738]
40. Kholmanskikh SS, Dobrin JS, Wynshaw-Boris A, Letourneau PC, Ross ME. Disregulated RhoGTPases and actin cytoskeleton contribute to the migration defect in Lis1-deficient neurons. J Neurosci. 2003; 23:8673–8681. [PubMed: 14507966]
41. Kholmanskikh SS, et al. Calcium-dependent interaction of Lis1 with IQGAP1 and Cdc42 promotes neuronal motility. Nat Neurosci. 2006; 9:50–57. [PubMed: 16369480]
42. Li H, Durbin R. Fast and accurate short read alignment with Burrows-Wheeler transform. Bioinformatics. 2009; 25:1754–1760. [PubMed: 19451168]

43. DePristo MA, et al. A framework for variation discovery and genotyping using next-generation DNA sequencing data. Nat Genet. 2011; 43:491–498. [PubMed: 21478889]
44. McKenna A, et al. The Genome Analysis Toolkit: a MapReduce framework for analyzing next-generation DNA sequencing data. Genome Res. 2010; 20:1297–1303. [PubMed: 20644199]
45. Cooper GM, et al. Single-nucleotide evolutionary constraint scores highlight disease-causing mutations. Nat Methods. 2010; 7:250–251. [PubMed: 20354513]
46. Grantham R. Amino acid difference formula to help explain protein evolution. Science. 1974; 185:862–864. [PubMed: 4843792]
47. Robinson JT, et al. Integrative genomics viewer. Nat Biotechnol. 2011; 29:24–26. [PubMed: 21221095]
48. Gilissen C, et al. Exome sequencing identifies WDR35 variants involved in Sensenbrenner syndrome. Am J Hum Genet. 2010; 87:418–423. [PubMed: 20817137]
49. Li H, et al. The Sequence Alignment/Map format and SAMtools. Bioinformatics. 2009; 25:2078–2079. [PubMed: 19505943]
50. Wang K, et al. PennCNV: an integrated hidden Markov model designed for high-resolution copy number variation detection in whole-genome SNP genotyping data. Genome Res. 2007; 17:1665–1674. [PubMed: 17921354]

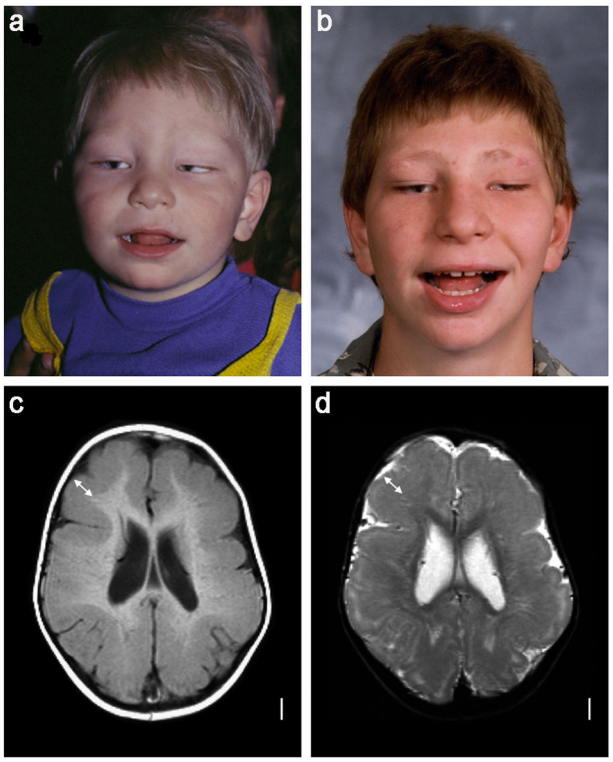

Figure 1.

Craniofacial appearance and magnetic resonance imaging (MRI) for patient LP92-083. Photos of patient at 2 years (**a**) and 17 years (**b**) show prominent metopic ridge or trigonocephaly (mid-forehead in **a**), high-arched eyebrows, ptosis, flat philtrum and wide mouth, and a suggestion of low-set ears. Brain MRI from T1- (**c**) and T2-weighted (**d**) images show abnormally wide cerebral convolutions and thick cortex (double arrows) in all regions, with the malformation more severe in anterior than in posterior regions. We obtained written consent to publish photographs of the patient.

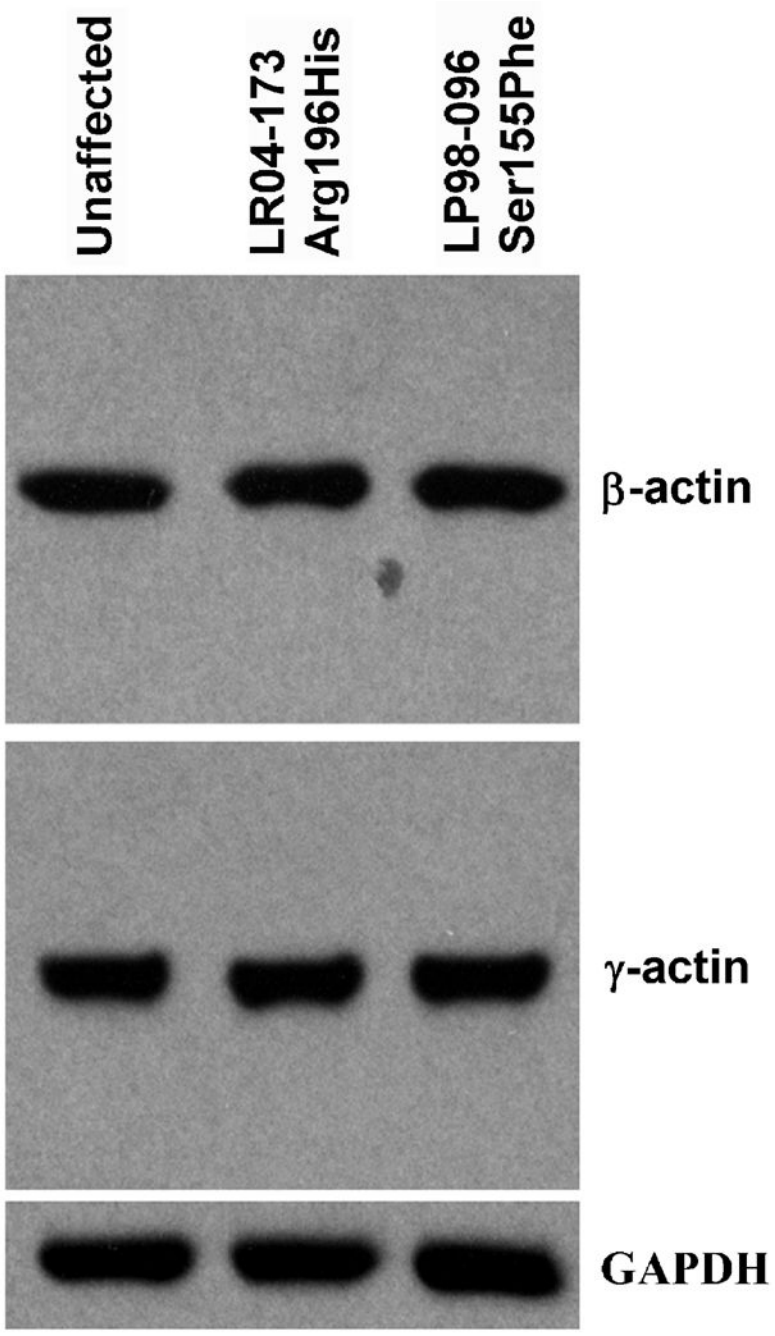

Figure 2.

Western Blot analysis of β- and γ-actin isoforms in lymphoblastoid cells derived from an unaffected control (line 09.1359) and two patients carrying the *ACTB* p.Arg196His (LR04-173) and *ACTG1* p.Ser155Phe (LP98-096) recurrent mutations using β-specific (Sigma clone AC-15) and γ-specific (Sigma clone 2–2.1.14.17) cytoplasmic actin antibodies. Protein extracts from cultured cells contained equal amounts of β- and γ-actin.

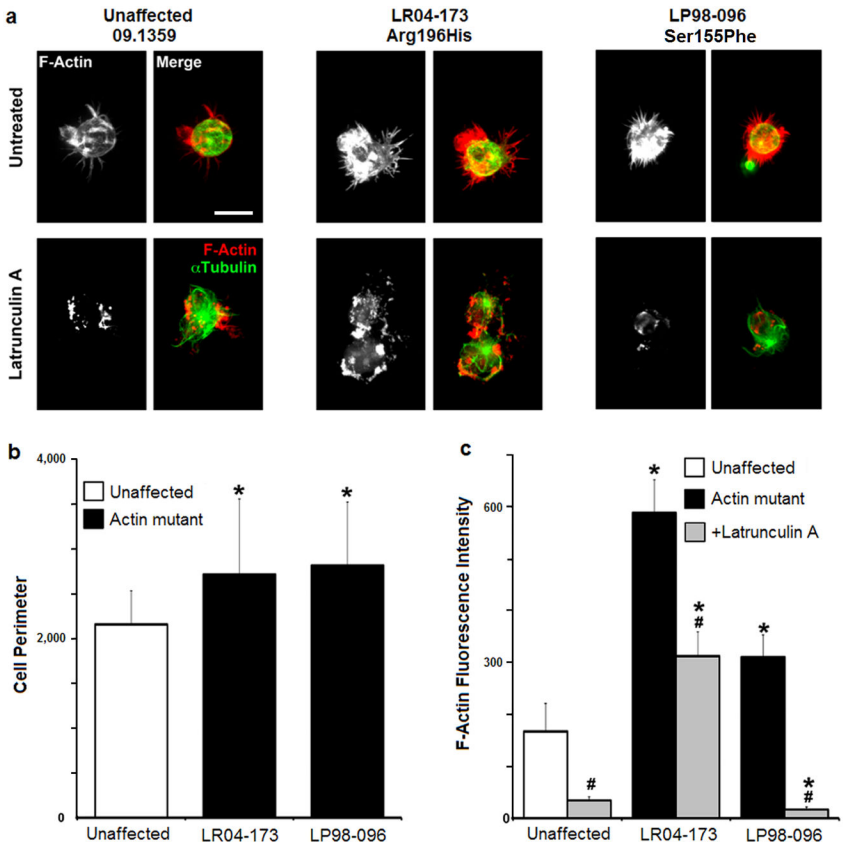

Figure 3.

Cytoskeletal organization, morphology and F-actin stability in lymphoblastoid cells derived from an unaffected control (line 09.1359) and two patients (LR04-173 and LP98-096). (**a**) Cells double-labelled for F-actin (red) and α-Tubulin (green). Mutant cells contain increased accumulations of F-actin, particularly around the nucleus (yellow in merged images) and in numerous filopodia-like protrusions. The scale bar corresponds to 10 μm. (**b**) Elaborate protrusions significantly increase the perimeter of mutant cells by 25–30% compared to control. (**c**) Quantification of phalloidin fluorescence intensity shows increased F-actin content (1.8 fold to 3.4 fold higher) in mutant compared to unaffected cells. Inhibition of actin polymerization by latrunculin A reduces F-actin in all cells, but while 20% of F-actin remains in normal cells, 55% of F-actin remains in β-actin-p.Arg196His cells, indicating more stabile F-actin, and only 5% remains in γ-actin-p.Ser155Phe cells, consistent with less stabile actin filaments associated with this mutation. * Statistically significant difference compared to untreated control cells 09.1359, # statistically significant difference compared to untreated cells of the same line ($p<0.05$, two-tail t-test assuming unequal variance, n=28 cells in each group). Error bars indicate standard deviation.

Table 1

Summary of the exome sequencing results from three probands with Baraitser-Winter syndrome

Family ID	Target size (Mb)[a]	Depth of coverage		Percent target covered at 10x	Total variants	Rare variants[b]	Candidate *de novo*
		Mean	Median				
LP92-083	36.7	78.5	61.0	88.33	22,591	256	2
58248	50.0	88.1	65.2	85.36	28,497	113	6
58431	50.0	88.5	67.3	90.25	29,685	131	3

Mb: Megabasepairs.

[a]Trio 1: SeqCap EZ Exome v2.0 (Roche). Trios 2 and 3: SureSelect Human All Exon 50Mb kit (Agilent).

[b]Trio 1: protein-altering and splice-site variants absent from dbSNP (build 132), 1000 Genomes Project data, and 101 other exomes. Trios 2 and 3: protein-altering and splice-site variants absent from dbSNP (build 132), 1000 Genomes Project data, and 332 other exomes.

Table 2

Summary of the *ACTB* and *ACTG1* mutations in 18 patients with Baraitser-Winter syndrome

Sample ID	Chr	Position (hg19)	Ref/alt alleles	Gene	cDNA change	Amino acid change	GERP score	Grantham score	CpG site	Inheritance	Other exomes[d]
LP98-085	7	5569255	T/C	*ACTB*	c.34A>G	p.Asn12Asp	4.45	23	N	De novo	0/24
LP90-050	7	5568962	G/C	*ACTB*	c.193C>G	p.Leu65Val	4.33	32	N	De novo	0/244
61456	7	5568128	G/A	*ACTB*	c.586C>T	p.Arg196Cys	0.5	180	Y	No parents	0/214
58248[a]	7	5568127	C/T	*ACTB*	c.587G>A	p.Arg196His	4.22	29	Y	De novo	0/212
59169	7	5568127	C/T	*ACTB*	c.587G>A	p.Arg196His	4.22	29	Y	De novo	0/212
LR04-173	7	5568127	C/T	*ACTB*	c.587G>A	p.Arg196His	4.22	29	Y	No parents	0/212
LR09-079	7	5568127	C/T	*ACTB*	c.587G>A	p.Arg196His	4.22	29	Y	No parents	0/212
LR06-298	7	5568127	C/T	*ACTB*	c.587G>A	p.Arg196His	4.22	29	Y	No parents	0/212
11-11287[b]	7	5568127	C/T	*ACTB*	c.587G>A	p.Arg196His	4.22	29	Y	No parents	0/212
11-10211	7	5568127	C/T	*ACTB*	c.587G>A	p.Arg196His	4.22	29	Y	No parents	0/212
61458	17	79478933	G/A	*ACTG1*	c.359C>T	p.Thr120Ile	4.16	89	N	De novo	0/244
LR06-241	17	79478612	G/A[c]	*ACTG1*	c.404C>T	p.Ala135Val	2.95	64	N	De novo	0/192
LR04-298	17	79478552	G/A	*ACTG1*	c.464C>T	p.Ser155Phe	4.25	155	N	De novo	0/224
LP98-096	17	79478552	G/A	*ACTG1*	c.464C>T	p.Ser155Phe	4.25	155	N	De novo	0/224
11-10857	17	79478552	G/A	*ACTG1*	c.464C>T	p.Ser155Phe	4.25	155	N	No parents	0/224
58431[a]	17	79478408	G/T	*ACTG1*	c.608C>A	p.Thr203Lys	3.11	78	N	De novo	0/203
LR03-033	17	79478256	G/A	*ACTG1*	c.760C>T	p.Arg254Trp	0.08	101	Y	De novo	0/195
LP92-083[a]	17	79478250	G/A	*ACTG1*	c.766C>T	p.Arg256Trp	1.6	101	Y	De novo	0/184

Abbreviations: Chr: chromosome. GERP: Genomic Evolutionary Rate Profiling.

[a] Patients from the whole-exome sequencing trios.

[b] Patient 11-11287 was originally diagnosed as having Fryns-Aftimos syndrome[16] (patient 1 in the original report, see Supplementary note for phenotype analysis).

[c] Variant reported in dbSNP (rs11549190).

[d] Presence of the mutations in 244 control exomes sequenced at the University of Washington (see **Online Methods** for details); Other exomes numerator: number of samples carrying the variant; denominator: total number of samples with base covered ≥ 8x.

Table 3

Clinical Overview of patients with Baraitser-Winter syndrome

	***ACTB* patients (n=10)**		***ACTG1* patients (n=8)**	
	Total numbers	**%**	**Total numbers**	**%**
Growth				
Short stature	6/10	60	3/7	42.9
Microcephaly, postnatal	6/9	66.7	4/7	57.1
Neurological				
Intellectual disability	9/9	100	5/5	100
Hearing loss	4/8	50	5/6	83.3
Seizures	9/9	100	7/8	87.5
Facial dysmorphism				
Trigonocephaly	8/10	80	7/7	100
Hypertelorism	10/10	100	7/8	87.5
High-arched eyebrows	10/10	100	7/7	100
Ptosis, congenital	10/10	100	8/8	100
Eyes				
Coloboma (iris or retina)	6/10	60	5/7	71.4
Lissencephaly type				
Pachygyria or pachygyria-band a>p	8/8	100	7/7	100

Gradient a>p: anterior greater than posterior lissencephaly. Total numbers columns: the numerator is the number of patients with the clinical feature; the denominator is the total number of patients for whom clinical data was available. See Supplementary Table 6 for a detailed, per patient, clinical overview.